RFID wireless system for detection of water in the annulus of a flexible pipe

F. Kuhn Matheus [*], P. Missell Frank, F. Borges Marcelo, G. R. Clarke Thomas

Physical Metallurgy Laboratory (LAMEF) PPGE3M/UFRGS - Universidade Federal do Rio Grande do Sul, Porto Alegre, Brazil

ARTICLE INFO

ABSTRACT

Corrosive environments are responsible for the highest degree of degradation and failure in marine structures. The presence of sea water in marine structures such as flexible pipes can cause a significant reduction in their operational life, especially when associated with permeated gases, which could lead to corrosion related failure mechanisms such as corrosion-fatigue and hydrogen cracking. The ingress of sea water into flexible pipes can occur either due to ruptures in their external polymeric sheath or to permeation of condensed water from the pipe bore. This event since flooding of the so-called annular space of flexible pipes is the trigger for all knows corrosion assisted failure modes, it is clear that a system that is able to reliably detect the presence of water in the structure is highly desirable. This work will describe a radio frequency identification (RFID) system designed for this purpose; it relies on the measurement of shifts in the resonance frequency of specially-designed tags which would be inserted within the layers of the flexible pipe during manufacturing. This paper shows the design and validation process of these tags and also of a reader which is meant to be scanned along the outside surface of the pipe by a remotely-operated vehicle (ROV). The study was performed through a finite element analysis and a test in which the tags were inserted within a full-scale mock-up of a flexible riser, which was then flooded with synthetic seawater. Results show that the shift in response due to sea water is clearly identifiable and distinguishable from other effects.

1. Introduction

Flexible pipes are marine structures in widespread use in off-shore exploration, production and transportation of oil and gas [1]. Their main function is connecting subsea production wells to floating processing and storage units present at sea level [2–4]. They are conventionally called risers when in the vertical position, or flow-lines when laying on the seabed, and are composed of multiple metallic and polymeric concentric layers, which are overlaid but independent of one another. Each layer has a specific function, the metallic ones being responsible for load-bearing whereas the polymeric ones act as barriers for internal and external fluids and gases [5–8]. Damage to the external polymeric layer can lead to the penetration of sea water into the annular region of the flexible pipe, which is defined as the space between the external and internal fluid barriers, as shown in Fig. 1. Water can also permeate through the polymeric barriers from the internal product. In any circumstance, flooding of this area leads to a shorter operational life due to corrosion related failure mechanisms. Furthermore, when flooding is combined with the stresses to which the structure is subjected because of waves and ocean currents, certain levels of CO_2, and high external pressure, stress corrosion cracking can occur,

---

* Corresponding author.
E-mail address: matheus.kuhn@ufrgs.br (F.K. Matheus).

accelerating even further the deterioration of the structure [9–11]. Thus, the detection of the presence of water in the annular region of these marine structures is an important piece of information for estimating their remaining life [12].

Determination of whether the annulus is flooded or not has been attempted in different manners, i.e. through the positive pressure or the vacuum tests, visual or ultrasonic inspection, or by fiber optics sensing [13–15]. The positive pressure and the vacuum tests require vents that connect to the annular region; often these tests do not produce accurate results or cannot be performed due to operational issues (i.e. vent blockage) [13,14]. Visual inspection can be used to encounter breaks in the outer sheath, but small abrasions or cuts can easily be missed along the vast extension of a riser. Ultrasonic methods are based on the attenuation of the signal when sea water is flooding the annular space [13]. However, the surface must be clean to allow sensor coupling, and the complex geometry of the structure can lead to misleading results. Distributed-sensing fiber optics systems are based on the presumption that cold sea water entering the structure may lead to a measurable temperature difference [13,15]. However, issues have been identified relating to loss of continuity of the optical fiber (which is inserted within the armor wires, along the structure) due to ruptures caused by the high mechanical loads involved in installation and operation, and to the fact that the temperature difference may be negligible and that temperature equilibrium may be achieved before detection is possible [13].

Another group of experimental techniques which have been deployed with great success in structural health monitoring (SHM) use radio frequency identification (RFID) tag antennas and sensors. These sensors have potential applications in SHM for marine structures because of their passive, wireless, simple, compact size, and multimodal nature [16]. RFID technologies are very sensitive to the environment in which they are deployed, and variations in their impedance or resonance frequency have been employed for sensing purposes [17–19]. In addition, systems with multiple resonance frequencies have been employed for characterization of depth and orientation of surface cracks in several systems [20,21]. Systems for characterizing RFID tags, such as network analyzers, may be used to verify the detuning caused by variations in the environment in which the sensor is operating, allowing i.e. the detection of humidity through the variation in the resonance of the equivalent LC circuit [22,23]. As mentioned, RFID sensors can be read wirelessly and can be passive and self-energize during reading, thus eliminating the need for batteries [24,25].

The objective of the present work is to detect flooding of the annular region of a flexible pipe by using RFID sensors operating at high frequencies (HF). This requires the possibility of developing small, flexible, low-cost sensors, which could operate passively during the entire useful life of the structure and which would detect changes in the conditions of the annular region, without the necessity of a chemical interaction or an electrical contact with the medium. It is also important to be able to identify the flooded region, while obtaining data with the insulating layers in place. The sensor tags might be inserted between the tensile armor and the external sheath during the manufacture of the pipe, although this solution could not be applied in flexible ducts already in operation. These tags would be positioned periodically along the length of the pipe and around its circumference. A requisite is that reading of the tags should be possible from the outer surface, through polymeric coatings of thicknesses up to 0.02 m. The attenuation generated by sea water is well known [26] so that, in this paper, the reader is considered to be placed directly onto the external sheath, as shown in Fig. 1. This demands a good maneuverability on the part of the ROV since the signal acquisition coil (reader) would be in near contact with the external sheath of the flexible pipe. Also, system response should be independent of temperature variations.
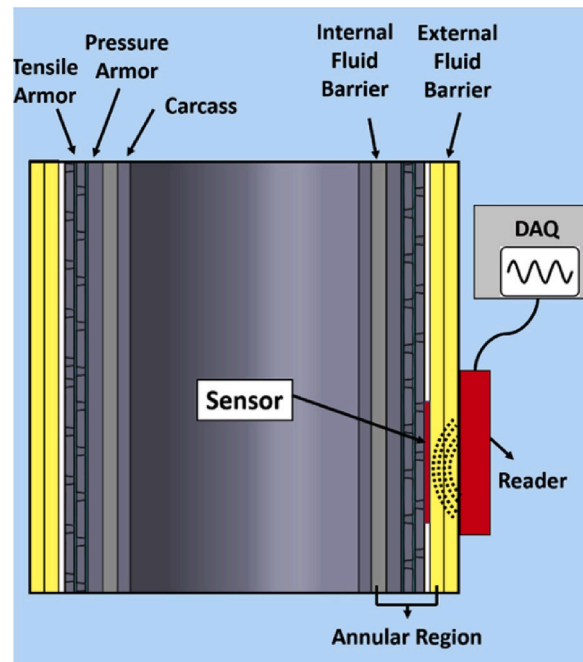

Fig. 1. Schematic showing a section of a flexible pipe with a RFID tag (sensor) inserted within its layers and a reader scanning the pipe from the outside surface. Tags should be inserted periodically within the layers of the pipe during manufacturing.

Finite Element Analysis (FEA) was carried out to design the reader and the sensors, and to verify the response of the system to changes in the environment. Relevant parameters, such as the coupling factor and the geometry were evaluated analytically and through FEA. In a second stage, an experimental study was carried out in a flexible pipe section under controlled conditions.

2. Materials and methods

2.1. System development

Wireless power transfer (WPT) systems are widely used and have diverse applications, one of which is RFID technology [27–29]. This technology employs inductive coupling to achieve data transfer [30,31]. The RFID system is composed of two components, a reader and a transponder or sensor. The reader is a coil which generates a RF signal, whereas the transponder or sensor is another coil that captures a fraction of this electromagnetic signal through current induction [32]. This fraction of the incident energy captured by the second coil can be represented by a coupling factor k. The value of the coupling coefficient can be given by Equation (1) for circular coils [33]. For systems in which the radius of the reader coil, r_r, is larger than or equal to the radius of the sensor coil, r_s, R is equal to r_r. For systems in which the radius of the reader coil is smaller than the radius of the sensor coil, R is equal to r_s. In this equation x is the distance between the two coils.

$$k = \frac{r_s^2 * r_r^2}{\sqrt{r_s * r_r} * \left(\sqrt{x^2 + R^2}\right)^3} \tag{1}$$

A coupling coefficient $k = 1$ is obtained when the distance between the coils is zero and both have the same radius. In this case both coils are exposed to exactly the same magnetic flux [32]. Fig. 2 presents the behavior of k as a function of reading distance for different relationships between the radius of the coils of the sensor and the reader. Note that for small distances the largest value of k for a given separation is achieved when the two coils have the same radius. For separation distances larger than about 0.035 m a sensor with a larger coil radius will lead to higher coupling coefficient values. The dashed lines in Fig. 2 indicate the distances corresponding to the thicknesses of the external barrier commonly employed in flexible pipes (single or double sheath). The figure shows that for these reading distances the diameter of the coils of the reader and the sensor should be the same.

Fig. 3 shows the variation of k with reading distance when sensor and reader coil radius are equal, for increasing values of diameter. These curves may suggest that maximizing the radii of the coils is always a good strategy, since this would lead to higher values for the coupling coefficient. However, the magnetic field strength needs to be taken into account. The magnetic field on the axis of a circular loop at a distance x is given by Equation (2), where I is the current and N the number of turns in the coil.

$$H = \frac{I.N.r_r^2}{2\sqrt{\left(r_r^2 + x^2\right)^3}} \tag{2}$$

Fig. 4 shows the variation of magnetic field and coupling factor with the radius of the reader and coil ($r_s = r_r$). The curves in solid lines represent the response considering a separation distance between coil and reader of one layer of external sheath, whereas dashed lines represent the response for a distance equal to two layers. As suggested by Fig. 3, increasing radii values lead to higher coupling factors. The magnetic field strength on the other hand reaches a maximum and then there is a reduction in the values for larger radii values. Considering that a single geometry of sensor and reader is wanted for both cases of external sheath thickness, an optimal point would be found when the radius of the reader and sensor coil are approximately equal to 0.0325 m, as indicated in Fig. 4.
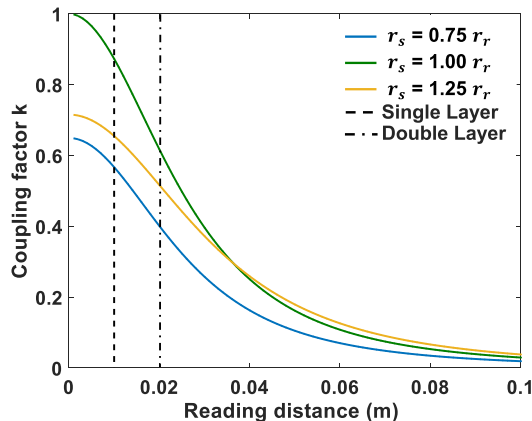

Fig. 2. Magnetic coupling coefficient as a function of reading distance for different relationships between the radii of the sensor coil (rs) and the reader coil (rr). Single Layer and Double Layer refer to the thickness of the polymeric sheath separating the reader and the sensor.
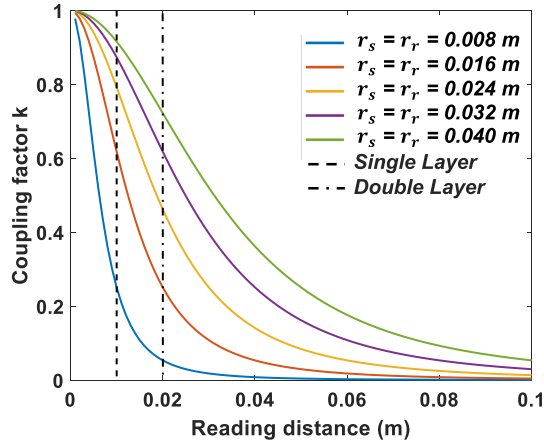
Fig. 3. Magnetic coupling coefficient as a function of reading distance and its relation to coil radius (rs = rr). Single Layer and Double Layer refer to the thickness of the polymeric sheath separating the reader and the sensor.
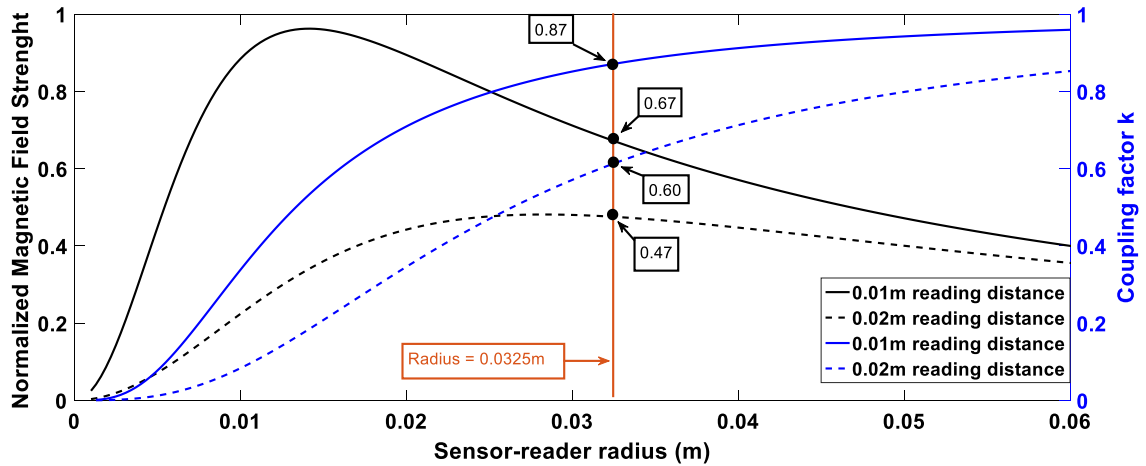

Fig. 4. Normalized magnetic field strength (black lines) and coupling factor (blue lines) as a function of the radius of the sensor and of the reader (rs = rr) for reading distances of 0.01 m (single layer external sheath) and 0.02 m (double layer external sheath). (For interpretation of the references to colour in this figure legend, the reader is referred to the Web version of this article.)

In addition to the dependence of the RFID system on the coupling factor and the magnetic field, another issue is the penetration depth, which conventionally is the depth to which an electromagnetic field penetrates into a material before its intensity is reduced to about 37% of its surface intensity value. The penetration depth is given by Equation (3) [34].

$$D_p = \frac{C\sqrt{\varepsilon_r'}}{2\pi f \varepsilon_r''} \tag{3}$$

where C is the wave velocity in the medium of application, ε_r' is the relative permittivity of the material, and ε_r'' is the loss factor of the material. This equation relates the frequency of operation, the properties of the material or medium situated between the reader and the sensor coils, as well as the coil separation, and must be considered in the development of the system. Since the desired application in this work is underwater, we note that the penetration distance for sea water with a conductivity of 4 S/m is 68 mm at 13.56 MHz [35]. In this way, since a possible water layer within the flexible pipe will be thinner than this penetration depth, one can assume that there will always be magnetic flux incidence upon the sensor. Detection would then rely on attenuation of the signal due to the electrical conductivity of the internal sea water layer. These attenuation values may be calculated through Equation (4) [35].

$$\alpha = 0.0173\sqrt{f\sigma} \tag{4}$$

In this equation f is the frequency of operation and σ is conductivity of the environment or material. For our selected frequency of 13.56 MHz, and considering a conductivity of 4 S/m, the attenuation value is 0.127 dB/mm [35].

Equation (3) and the calculated penetration depth in sea water given above also mean that the reader should be as close as possible to the external sheath in order to minimize losses to the external sea water medium. This reading distance should also be kept constant in order to reduce the influence of variations in thickness of the external sea water layer on the response of the system. It is thought that the best way to achieve this is to have direct contact between the reader and the external surface of the pipe.

Another issue is that RFID tags, when operating with inductive coupling, and when applied directly over a metallic surface tend to have a poorer performance [36]. This is because when fractions of the magnetic flux generated by the RFID system interact with a substrate metal, eddy currents are induced, which produce a field contrary to the primary magnetic field and therefore contrary to the field produced by the reader coil. This reduces the useful distance of the system, leading to a change in the inductance and therefore the resonance frequency of the

system [37,38]. Inserting a high permeability material like ferrite between the reader coil and the metallic substrate could reduce drastically the generation of eddy currents [33,39]. However, when this additional layer is used, the inductance of the sensor coil increases significantly [33] and this influences the frequency-response and resonance frequency of the sensor; hence, the geometry of the system must be adjusted to guarantee an adequate impedance matching. This effect was evaluated through finite element modelling studies.

The sensitivity of the system to environmental changes derives from the detection of shifts in the resonance frequency of its equivalent circuit, that can be defined by Equation (5) [40]. When there is an alteration in the medium in which the sensor is deployed the dielectric constant changes, leading to a change in the value of the capacitor C_a, thus altering the equivalent capacitance of the circuit, C_e, given in Equation (6), and finally of the resonance frequency of the circuit.

$$f_0 = \frac{1}{2\pi\sqrt{C_e L_a}} \tag{5}$$

$$C_e = C_C + C_a \tag{6}$$

2.2. Finite element modelling - FEM

Ansys HFSS was used to perform finite element simulations of the system. The geometry proposed for both the reader and sensor coils is that of a planar coil, since this geometry is flat and therefore can be applied between the layers of the flexible pipe. The aim is to obtain a sensor which is resonant at 13.56 MHz when the annular region is flooded, which is the most critical situation, and one that will guarantee communication between the RFID component and the reader electronics. The dimensions of the reader and sensor coils are given in Table 1.

This FEM study allowed the design and characterization of the system, and to establish the influence of several issues on its frequency-response. These were:

- the effect of proximity to the metallic substrate (flexible riser armor wires) and the effect of adding an intermediate ferrite layer.
- the effect of water layer thickness. For this, models were built with and without a 0.7 mm-thick layer of water between the sensor and the metallic substrate. A water gap of 0.7 mm was also considered between the reader and the external fluid barrier.
- the effect of the thickness of an insulating coating which is applied to the sensors.
- the influence of sea water conductivity. This is because the conductivity of sea water can vary with depth, and also because the sensor will be positioned in a confined space in which different salt concentrations may occur.

In the numerical model of the inductively coupled coils, a lumped port with 50 Ω was considered for the excitation source and the RFID component was modeled as a lumped element with 50 pF. Two types of elements were used, prismatic for the FR4 substrate and tetrahedric for the polyamide, metallic substrate and water layers. All of the contacts between the copper lines and the medium were considered to be shielded from water. The properties of the materials used in the model are presented in Table 2.

2.3. Experimental testing

The reader and sensor coils were produced from a substrate of FR4 with a thickness of 0.2 mm and a 35 μm-thick copper layer. The fabrication process was carried out using a LPKF Protomat S63 milling machine. The RFID component used in this work was NT3H2111_2211, produced by NXP, with an internal capacitance of 50 pF at 13.56 MHz, in accordance with ISO/IEC 14443. The RFID component was soldered in place. A sheet of flexible sintered ferrite with dimensions 120 mm × 120 mm, WE-FSFS 364003, was

Table 1
Sensor and reader coil dimensions.

Parameter	Sensor Coil	Reader Coil
Conductor Width	0.5 mm	0.5 mm
Conductor Spacing	0.2 mm	–
Inner Radius	30 mm	32 mm
Turns	3	1
Substrate Thickness	0.2 mm	0.2 mm

Table 2
Material properties used in numerical models.

Material	Relative Permeability	Relative Permittivity	Electrical Conductivity (S/m)	Loss Tangent
Air	1.0006	1.0000004	0	0
Copper	1	1	5.998e7	0
Sea Water	0.999991	81	4	70
Polyamide	1	4.3	0	0.004
Ferrite	120	12	0	0
FR4	1	4.5	0	0.02
Steel	1000	1	4.032e6	0

positioned on the backside of the FR4. All of the electrical contacts were isolated using polyurethane, PU-140.

The process of identifying the sensor was carried out with a conventional RFID reader. The shift in the resonance frequency value was determined with a Vector Network Analyzer (National Instruments PXIe_5630), which allows one to measure the S11 parameter wirelessly. The frequency was swept from 10 MHz to 20 MHz in steps of 0.01 MHz (1000 points). The calibration of the equipment was carried out using an Automatic VNA Calibration Kit (National Instruments, operating bandwidth from 70 kHz to 9 GHz).

Two tests were performed in this experimental section. In the first test, windows were opened in the external sheath of a 1.5m-long flexible pipe section in order to allow insertion of 4 RFID sensors. Resistive sensors were also placed in these windows to detect the presence of water independently. Fig. 5 shows the pipe segment with the open windows. After positioning the sensors, the layers of polymer which had been removed were replaced and soldered in order to guarantee the structure to be water tight. The sample pipe was placed within an acrylic recipient which could be subsequently filled with synthetic sea water (according to the standard ASTM D1141-98).

Initially the sensors were identified in their dry condition through their unique RFID and then measurements of S11 and the resonance frequency were made. After collecting this data, the annular region was flooded and data was recollected for this new configuration. Fig. 6 presents the configuration of the tests.

A second test consisted in evaluating the variation of the signal with temperature. For this, a sensor and a reader were placed inside a temperature chamber (SOLAB SL-206) and data was collected in the interval from 5 °C until 55 °C. This is the temperature range encountered at the sensor position in flexible risers [41,42] and for sea water at great depths.

3. Results

3.1. Finite element modelling

Fig. 7 shows the effect of the proximity of the metallic substrate on the resonance frequency and the signal intensity (S11 modulus in dB) of the system with and without a ferrite interlayer. The figure shows that in the case where a ferrite interlayer is not used there is increase in the resonance frequency as well as a considerable reduction in the signal intensity for smaller distances. The addition of a

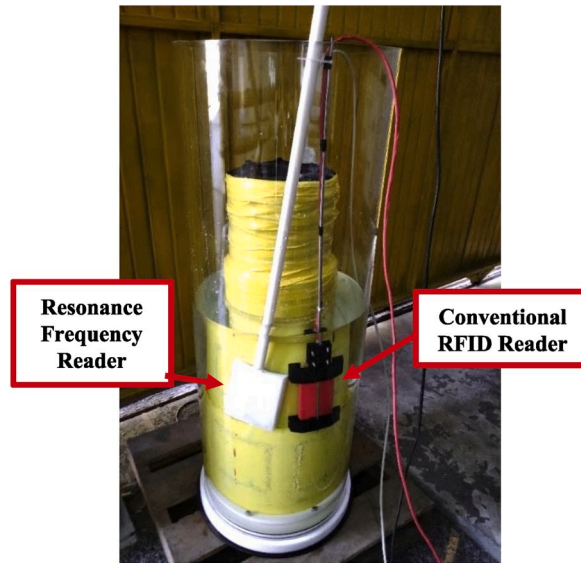**Fig. 5.** Segment of the flexible pipe with openings for the insertion of sensors.

Fig. 6. Configuration of the test with external sea water container.
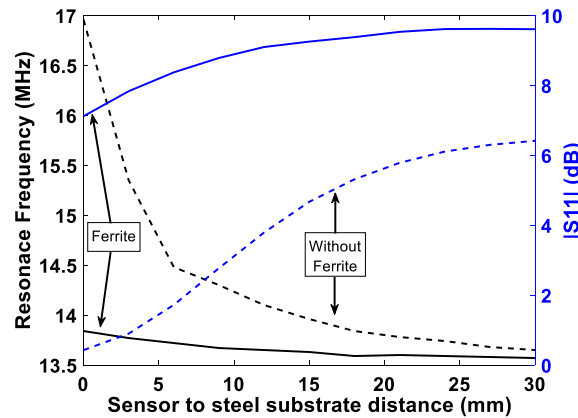

Fig. 7. Resonance frequency and S11 modulus as a function of distance of the sensor coil to a steel substrate. Solid lines consider a ferrite backplate of 0.3 mm in between the sensor and the steel substrate, and dotted lines are for no-backplate condition.

0.3 mm-thick ferrite layer between the sensor and the metallic surface reduces both the variations in the resonance frequency and the variations in the signal intensity.

The results for the numerical modelling of the effect of water flooding can be seen in Fig. 8. The resonance frequency for the flooded annular condition using Ansys HFSS was of 13.50 MHz and 14.69 MHz for the dry condition. The models show a marked shift in the resonance frequency to lower values and an attenuation of the S11 parameter when the pipe is flooded.

The results for the effect of the thickness of a sensor coating layer can be seen in Fig. 9. One can see that there is a reduction in the resonance frequency variation as the thickness increases, which is evidently due to the smaller interaction between the sensor and the water medium for thicker coatings. Fig. 9 shows that when both sides of the sensor are covered with water there is a difference in the shift in the resonance frequency compared to when only the coil side is wet. For the sensors built for validation tests, the average of thickness obtained was of 0.13 mm.

The influence of the conductivity of sea water was also verified (from 2 to 6 S/m). The variation in the value of resonance frequency was smaller than the 0.025 MHz frequency step used in frequency-response sweeps. Small alterations were observed in the S11 modulus, of around 0.28 dB, a value which is significantly smaller that the variation for wet or dry conditions.

3.2. Experimental characterization and validation of the sensor

Fig. 10 shows results for the full-scale test, and shows that all four sensors had clear resonance frequency shifts during flooding. S11
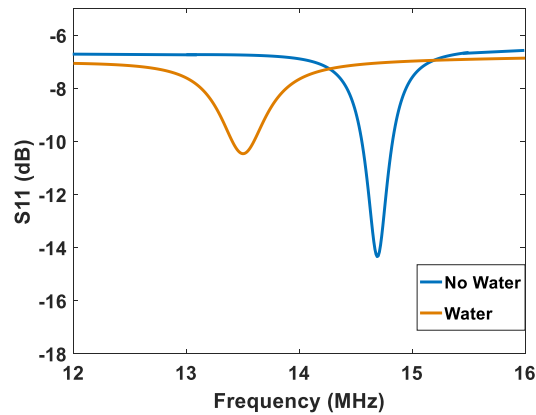
Fig. 8. Frequency-response of the system for dry and wet conditions, simulated results.
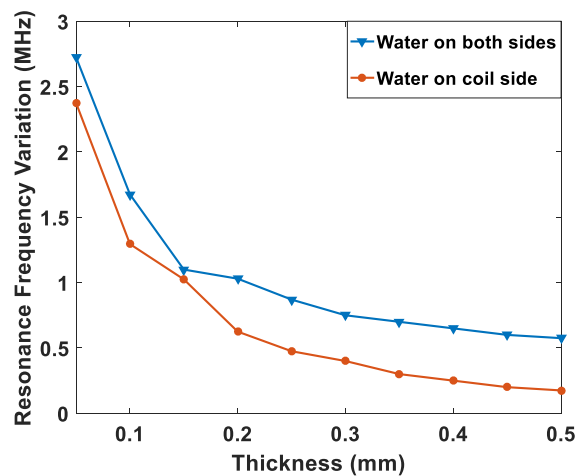

Fig. 9. Influence of thickness of polymer coating on resonance frequency shift, simulation results.

response in both dry and flooded conditions is similar to predictions from HFSS models in Fig. 8. Table 3 shows the results of resonance frequency shifts for the other sensors which were inserted in the pipe section. Fig. 10 also shows the influence of polymeric layer thickness on the S11 signal. For sensors positioned where one polymeric layer is present the magnitude of the parameter S11 is greater than for sensors in the double layer region. This effect is expected and is related to the reduction in magnetic field strength due to the distance between coils.

Fig. 11 shows the shift in resonance frequency from dry to flooded condition for sensor ID 2049022468. As the external sea water container was removed and the pipe section was allowed to dry, it is seen that in about three days the resonance frequency value was close to being reestablished to the previous dry value.

A second test consisted in measuring the change in frequency-response with temperature; these results are presented in Fig. 12. Three measurement were taken at each temperature value for the same sensor and reader configuration; good repeatability is seen in the measurements. It is also seen that for a temperature variation of about 50 °C the resonance frequency shift is approximately 4 times smaller than the variation in resonance frequency caused by water. It should be noted that in subsea applications, temperatures shifts are expected to be small since external sea water temperatures and internal product temperatures are relatively constant.

4. Conclusion

The effectiveness of the detection of flooding in the annular region of flexible pipes using RFID sensors operating at high frequencies has been demonstrated. Significant and characteristic variations in the resonance frequency of the system were observed when the annular region was flooded, thus allowing the possibility of detection of the presence of water in these structures. The sensors were shown to be able to recover to their previous response once the annulus has dried, although this is unlikely to happen in practice
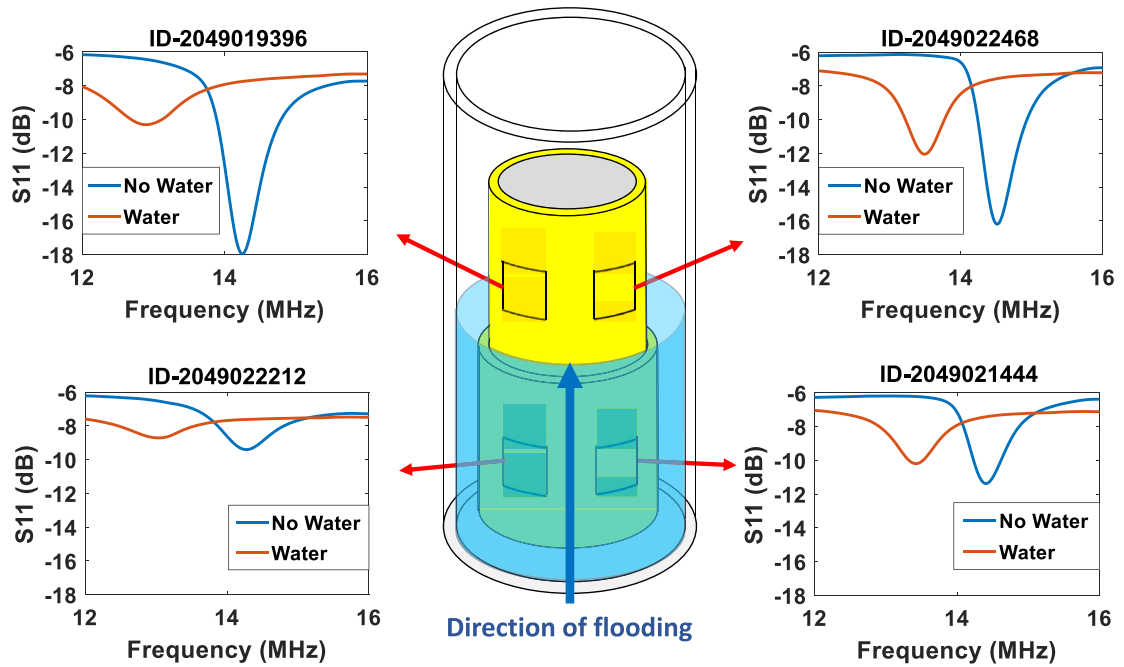
Fig. 10. Frequency-response of the system for dry and wet conditions, experimental results.

Table 3
Resonance frequency values for dry and wet conditions for the 4 sensors distributed throughout the flexible pipe.

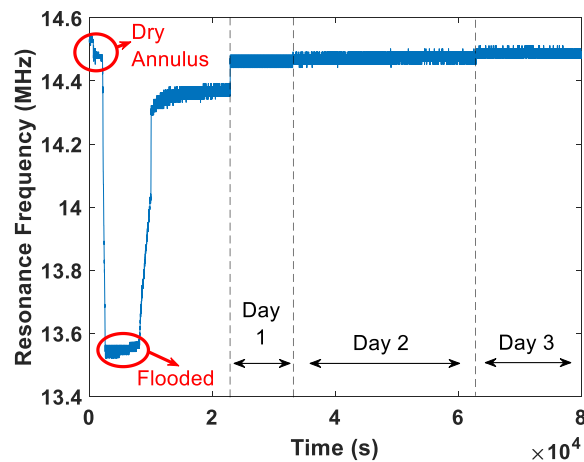| Sensor ID	Frequency Dry (MHz)	Frequency with Water (MHz)	Frequency Variation (MHz)
2,049,021,444	14.41 ± 0.025	13.42 ± 0.055	1.01
2,049,022,468	14.49 ± 0.009	13.53 ± 0.021	0.96
2,049,022,212	14.26 ± 0.011	13.02 ± 0.078	1.24
2,049,019,396	14.24 ± 0.012	12.88 ± 0.136	1.36

Fig. 11. Resonance frequency change as a function of time throughout a flooding and drying cycle, experimental results.

in flexible risers. The effect of temperature on the sensor signal was measured and can be considered negligible for the temperature shifts expected for subsea applications.

The system is shown to be capable of easily detecting flooding in these marine structures even when they are covered by two layers of polymeric insulation. Signal acquisition is possible even for greater distances, but with a corresponding loss in signal intensity.
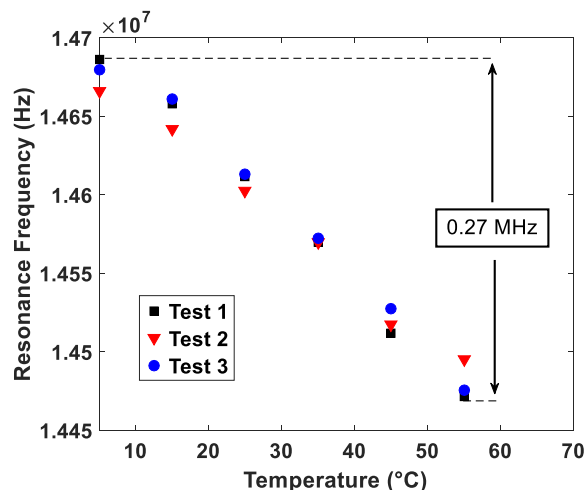
Fig. 12. Influence of temperature on the resonance frequency of the sensor, experimental results.

Declaration of competing interests

The authors declare that they have no known competing financial interests or personal relationships that could have appeared to influence the work reported in this paper.

Acknowledgements

References

[1] Lukassen TV, Gunnarsson E, Krenk S, Glejbøl K, Lyckegaard A, Berggreen C. Tension-bending analysis of flexible pipe by a repeated unit cell finite element model. Mar Struct 2019;64:401–20. https://doi.org/10.1016/j.marstruc.2018.09.010.
[2] Fang P, Yuan S, Cheng P, Bai Y, Xu Y. Mechanical responses of metallic strip flexible pipes subjected to pure torsion. Appl Ocean Res 2019;86:13–27. https://doi.org/10.1016/j.apor.2019.02.009.
[3] Yoo DH, Jang BS, Yun RH. A simplified multi-layered finite element model for flexible pipes. Mar Struct 2019;63:117–37. https://doi.org/10.1016/j.marstruc.2018.08.006.
[4] Bai Q, Bai Y, Ruan W. Flexible pipes: advances in pipes and pipelines. John wiley & sons. Page 3, ISBN 978-1-119-04126-9.
[5] Tang M, Lu Q, Yan J, Yue Q. Buckling collapse study for the carcass layer of flexible pipes using a strain energy equivalence method. Ocean Eng 2016;111:209–17. https://doi.org/10.1016/j.oceaneng.2015.10.057.
[6] Mac DH, Sicsic P. Uncertainties propagation within offshore flexible pipes risers design. Procedia engineering 2018;213:708–19. https://doi.org/10.1016/j.proeng.2018.02.067.
[7] Vaz MA, Rizzo NAS. A finite element model for flexible pipe armor wire instability. Mar Struct 2011;24(3):275–91. https://doi.org/10.1016/j.marstruc.2011.03.001.
[8] Li X, Jiang X, Hopman H. Predicting the wet collapse pressure for flexible risers with initial ovalization and gap: an analytical solution. Mar Struct 2020;71:102732. https://doi.org/10.1016/j.marstruc.2020.102732.
[9] Popoola LT, Grema AS, Latinwo GK, Gutti B, Balogun AS. Corrosion problems during oil and gas production and its mitigation. Int J Integrated Care 2013;4(1):35. https://doi.org/10.1186/2228-5547-4-35.
[10] Ossai CI, Boswell B, Davies IJ. Pipeline failures in corrosive environments–A conceptual analysis of trends and effects. Eng Fail Anal 2015;53:36–58. https://doi.org/10.1016/j.engfailanal.2015.03.004.
[11] Revie RW, editor. Oil and gas pipelines: integrity and safety handbook. John Wiley & Sons; 2015. p. 78.
[12] Netto TA, Honorato HJ, Qassim RY. Prioritization of failure risk in subsea flexible pipes via data envelopment analysis. Mar Struct 2013;34:105–16. https://doi.org/10.1016/j.marstruc.2013.08.001.
[13] Nott P, Shepherd W, McNab J, Harley P, Ahmed SZ. June). A novel electrical based breach detection system for flexible pipe. In: ASME 2016 35th international conference on ocean, offshore and arctic engineering. American Society of Mechanical Engineers; 2016. https://doi.org/10.1115/OMAE2016-54781. V005T04A016-V005T04A016.
[14] Bondevik JO, Lunde S, Haakonsen R. January). Annulus testing for condition assessment and monitoring of flexible pipes. In: ASME 2004 23rd international conference on offshore mechanics and arctic engineering. American Society of Mechanical Engineers; 2004. p. 763–8. https://doi.org/10.1115/OMAE2004-51431.
[15] Dahl CS, Andersen BAM, Gronne M. January). Developments in managing flexible risers and pipelines, a suppliers perspective. In: Offshore technology conference. Offshore technology conference; 2011. https://doi.org/10.4043/21844-MS.
[16] Zhang J, Tian GY, Marindra AM, Sunny AI, Zhao AB. A review of passive RFID tag antenna-based sensors and systems for structural health monitoring applications. Sensors 2017;17(2):265. https://doi.org/10.3390/s17020265.
[17] Potyrailo RA, Mouquin H, Morris WG. Position-independent chemical quantitation with passive 13.56-MHz radio frequency identification (RFID) sensors. Talanta 2008;75(3):624–8. https://doi.org/10.1016/j.talanta.2007.06.023.
[18] Kuhn MF, Breier GP, Dias ARP, et al. J Nondestr Eval 2018;37:22. https://doi.org/10.1007/s10921-018-0475-3.
[19] Kuhn MF, Jacques RC, Clarke TGR. J Nondestr Eval 2019;38:60. https://doi.org/10.1007/s10921-019-0598-1.

[20] Marindra AMJ, Tian GY. Chipless RFID sensor tag for metal crack detection and characterization. IEEE Trans Microw Theor Tech 2018;66(5):2452–62. https://doi.org/10.1109/TMTT.2017.2786696.

[21] Daura LU, Tian GY. Wireless power transfer based non-destructive evaluation of cracks in aluminum material. IEEE Sensor J 2019;19(22):10529–36. https://doi.org/10.1109/JSEN.2019.2930738.

[22] Ong KG, Grimes CA, Robbins CL, Singh RS. Design and application of a wireless, passive, resonance-circuit environmental monitoring sensor. Sensor Actuator Phys 2001;93(1):33–43. https://doi.org/10.1016/S0924-4247(01)00624-0.

[23] Harpster TJ, Stark B, Najafi K. A passive wireless integrated humidity sensor. Sensor Actuator Phys 2002;95(2–3):100–7. https://doi.org/10.1016/S0924-4247(01)00720-8.

[24] Islam T, Mahboob MR, Khan SA, Kumar L. A single chip integrated sol-gel thin film LC sensor for measuring moisture in ppm level. IEEE Sensor J 2013;14(4):1148–53. https://doi.org/10.1109/JSEN.2013.2294336.

[25] Xie MZ, Wang LF, Dong L, Deng WJ, Huang QA. Low cost paper-based LC wireless humidity sensors and distance-insensitive readout system. IEEE Sensor J 2019. https://doi.org/10.1109/JSEN.2019.2901004.

[26] Benelli G, Pozzebon A. RFID under water: technical issues and applications. In Radio frequency identification from system to applications. InTechOpen 2013. https://doi.org/10.5772/53934.

[27] Ng DWK, Duong TQ, Zhong C, Schober R, editors. Wireless information and power transfer: theory and practice. Wiley-IEEE Press; 2019.

[28] Kim KY. Wireless power transfer-principles and engineering explorations. 2012.

[29] Lu Y, Ki WH, SpringerLink (Online service). CMOS integrated circuit design for wireless power transfer. Springer; 2018.

[30] Chawla V, Ha DS. An overview of passive RFID. IEEE Commun Mag 2007;45(9):11–7.

[31] Reinhold C, Scholz P, John W, Hilleringmann U. Efficient antenna design of inductive coupled RFID-systems with high power demand. J Commun 2007;2(6):14–23.

[32] Bolic M, Simplot-Ryl D, Stojmenovic I, editors. RFID systems: research trends and challenges. John Wiley & Sons; 2010.

[33] Finkenzeller K. RFID handbook: fundamentals and applications in contactless smart cards, radio frequency identification and near-field communication. John Wiley & Sons; 2010.

[34] Mehdizadeh M. Microwave/RF applicators and probes: for material heating, sensing, and plasma generation. William Andrew; 2015pp15.

[35] Giuliano Benelli and Alessandro Pozzebon. RFID under water: technical issues and applications, radio frequency identification from system to applications. Mamun Bin Ibne Reaz, IntechOpen; 2013. https://doi.org/10.5772/53934.

[36] Zhu H, Lai S, Dai H. Solutions of metal surface effect for hf rfid systems. In: 2007 international conference on wireless communications, networking and mobile computing. IEEE; 2007, September. p. 2089–92.

[37] Qing X, Chen ZN. Characteristics of a metal-backed loop antenna and its application to a high-frequency RFID smart shelf. IEEE Antenn Propag Mag 2009;51(2):26–38.

[38] Qing X, Chen ZN. Proximity effects of metallic environments on high frequency RFID reader antenna: study and applications. IEEE Trans Antenn Propag 2007;55(11):3105–11. https://doi.org/10.1109/TAP.2007.908575.

[39] Lee W, Hong YK, Park J, Lee J, Baek IS, Hur NP, Park SO. A simple wireless power charging antenna system: evaluation of ferrite sheet. IEEE Trans Magn 2017;53(7):1–5. https://doi.org/10.1109/TMAG.2017.2676099.

[40] Niu S, Matsuhisa N, Beker L, et al. A wireless body area sensor network based on stretchable passive tags. Nat Electron 2019;2:361–8. https://doi.org/10.1038/s41928-019-0286-2.

[41] Liu J, Vaz MA. Viscoelastic axisymmetric structural analysis of flexible pipes in frequency domain considering temperature effect. Mar Struct 2016;50:111–26. https://doi.org/10.1016/j.marstruc.2016.07.003.

[42] de Lima HF, Vaz MA, da Costa MF, Gomez AA, de Oliveira GL. Creep behavior of in-service flexible flowline polyamide 11. Polym Test 2020;81:106205. https://doi.org/10.1016/j.polymertesting.2019.106205.